

Article

Enhanced Nitrate Nitrogen Removal from Wastewater Using Modified Reed Straw: Adsorption Performance and Resource Utilization

Haodong Zhang ¹, Zhan Yang ¹, Jiawang Tian ¹, Changyi Liu ¹ and Zhe Qin ^{1,2,*}

¹ Hebei Key Laboratory of Close-to-Nature Restoration Technology of Wetlands, School of Eco-Environment, Hebei University, Baoding 071002, China; zhanghd@163.com (H.Z.); yangzhan531@163.com (Z.Y.); tianjiawang97@163.com (J.T.); l_ccccc@163.com (C.L.)

² Engineering Research Center of Ecological Safety and Conservation in Beijing-Tianjin-Hebei, Xiong'an New Area of MOE, Xiongxian 071800, China

* Correspondence: qinzhe945@163.com

Abstract: This paper presents a study on the efficient removal of nitrate nitrogen from wastewater using modified reed straw (MRS) and its subsequent resource utilization. The modification of the reed straw involved the introduction of branching quaternary amine groups to enhance its adsorption capacity for nitrate nitrogen. Experimental investigations were conducted to analyze the impact of packing height, flow rate, and initial solution concentration on the dynamic adsorption performance of the MRS. The results revealed that the maximum dynamic adsorption capacity of the MRS for nitrate nitrogen reached 14.76 mg/g. Furthermore, valuable nitrate nitrogen nutrient solution was successfully recovered through subsequent desorption experiments for resource recycling. Moreover, the application of the MRS led to notable enhancements in column height, fresh weight, chlorophyll content, and nitrogen content of the treated plants, indicating its efficacy in promoting plant growth. Overall, the findings demonstrate that MRS serves as a versatile adsorbent capable of efficient nitrate nitrogen removal and subsequent resource utilization.



Citation: Zhang, H.; Yang, Z.; Tian, J.; Liu, C.; Qin, Z. Enhanced Nitrate Nitrogen Removal from Wastewater Using Modified Reed Straw: Adsorption Performance and Resource Utilization. *Sustainability* **2024**, *16*, 4001. <https://doi.org/10.3390/su16104001>

Academic Editors: Gujie Qian, Yan Zhou and Weifeng Chen

Received: 3 April 2024
Revised: 26 April 2024
Accepted: 2 May 2024
Published: 10 May 2024



Copyright: © 2024 by the authors. Licensee MDPI, Basel, Switzerland. This article is an open access article distributed under the terms and conditions of the Creative Commons Attribution (CC BY) license (<https://creativecommons.org/licenses/by/4.0/>).

Keywords: adsorption and desorption; modified reed straw; resource utilization

1. Introduction

Nitrate is widely acknowledged as a prominent pollutant in surface and groundwater on a global scale [1]. The main sources of nitrate pollution include excessive use of fertilizers in agriculture, animal manure, atmospheric nitrogen deposition, and industrial discharges that produce nitrogenous wastewater [2,3]. At high concentrations, nitrate (NO_3^-) anions can pose potential toxicity risks. In biological systems, bacteria in the digestive system, particularly in the mouth and stomach, convert NO_3^- into NO_2^- ions [1]. These ions can react with hemoglobin in the blood, forming methemoglobin, ultimately leading to hypoxia [4]. Elevated levels of nitrates in drinking water can also have adverse effects on human health, particularly in infants and the elderly [5]. Numerous studies have demonstrated that prolonged exposure to high levels of nitrates and nitrites, especially through the consumption of processed meats, is associated with the development of colorectal cancer [6]. Additionally, the proliferation of algae and aquatic plants due to elevated concentrations of NO_3^- in freshwater sources can exacerbate eutrophication [7]. This phenomenon entails an excessive influx of nutrients into the water, fostering the rapid growth of algae and plants. Consequently, the increased organic matter decomposition consumes oxygen, leading to hypoxia or anoxia, which can detrimentally impact the survival of fish and other aquatic organisms [8].

Considering the serious health effects of high NO_3^- concentrations in drinking water, the World Health Organization has set a limit of 40 mg/L for NO_3^- ions in drinking wa-

ter [9]. Therefore, it is important to appropriately reduce NO_3^- levels in water and develop methods to remove these anions in order to comply with applicable regulations [10].

In current practices, the primary techniques employed for the removal of NO_3^- from wastewater include biological treatment and physicochemical methods, respectively [11]. Comparatively, these conventional treatments, such as nitrification, denitrification, and catalysis, involve intricate processes and generate challenging-to-dispose secondary byproducts [3,12]. As a result, adsorption has garnered significant interest due to its simplicity and lack of sludge production [13]. Numerous materials, such as natural adsorbents, miscellaneous adsorbents, and agricultural waste, can be employed for adsorption purposes. Agricultural waste, in particular, has garnered considerable attention due to its cost-effectiveness, facile preparation, and remarkable regenerability [14]. Nevertheless, while several studies have focused on the adsorption of NO_3^- onto various materials, the utilization of nitrogen post-adsorption has received minimal attention from researchers [14–17].

Reeds, belonging to the perennial aquatic or wet grass family, are abundant in fiber and have a wide distribution across Asia and Europe [18]. In the past, reed straw has been widely used in various inland aquatic ecosystems for nutrient removal. Its natural filtration and adsorption properties make it an ideal ecological engineering material for improving water quality and ecological balance. By adsorbing and absorbing nutrients in water, such as nitrogen and phosphorus, reed straw can effectively reduce the nutrient salt content in water, thereby preventing eutrophication and excessive algae growth in water bodies. However, their prolific and rapid reproductive methods have led to reed overgrowth, resulting in ecological damage in certain regions [19]. The conventional approach to addressing this issue involves direct burning of reed plants, yet this method entails significant environmental pollution and resource wastage [20]. Conversely, reeds have found diverse applications, including their use in capacitors [20], photocatalysis [21], and various adsorption studies. For instance, they have been employed in the removal of short-chain perfluoroalkyl acids [22], microcystins [23], as well as dyes and heavy metals [24].

In this work, we undertook the quaternization and modification of reed straw to synthesize modified reed straw (MRS), specifically targeting improved nitrate nitrogen adsorption from wastewater. Through comprehensive material characterization and analysis, we further assessed its adsorption performance for nitrate nitrogen. Building on these findings, we harnessed the material to concentrate and enrich nitrate nitrogen in wastewater via dynamic adsorption and desorption, resulting in a nitrogen-enriched nutrient solution suitable for subsequent resource utilization. Furthermore, we explored the material's impact on plant growth, aiming to establish a closed-loop resource utilization system. The results demonstrate the significant potential of MRS for effective nitrate removal and resource recovery.

2. Materials and Methods

2.1. Materials

The reed straws used in the experiment were obtained from Baiyangdian, Xiongan New Area, China. NaOH, anhydrous ethanol, was purchased from Tianjin Huihang Chemical Technology Co. Epichlorohydrin, N, N-dimethylformamide (DMF), SiO_2 , and KNO_3 were bought from Tianjin Komeo Chemical Reagent Co. KCl and boric acid were purchased from Fuchen (Tianjin) Chemical Reagent Co. Trimethylamine was bought from Shanghai McLean Biochemical Technology Co.

2.2. Synthesis of MRS

The collected reed straw (RS) was sun-dried, physically crushed, and sieved through a 60-mesh sieve to obtain RS powder. The RS powder underwent three washes with tap water and distilled water before being dried in an 80 °C oven. For pretreatment, 4.0 g of cleaned RS was immersed in 100 mL of 5 mol/L sodium hydroxide solution, stirred for 2 h at 25 °C, and then rinsed repeatedly with deionized water until the solution became colorless. Subsequently, it was dried in an 80 °C oven. In the modification process, 2.0 g

of the pretreated RS material was placed in a 1000 mL three-necked flask. Under 80 °C water-bath heating, 10 mL of epichlorohydrin and 20 mL of N,N-dimethylformamide were sequentially added, followed by stirring for 30 min. Then, 20 mL of trimethylamine was added into the flask, and the reaction continued for another 30 min. The modified material was washed three times with anhydrous ethanol and deionized water, then dried in an 80 °C oven until it reached a constant weight, resulting in the production of the modified reed straw (MRS) adsorbent.

2.3. Experimental Procedure

2.3.1. Characterization of MRS

The RS, MRS, and MRS-NO₃⁻ utilized in the experiments underwent comprehensive characterization and analysis. The microscopic morphology of each material was scrutinized using a scanning electron microscope (SEM) from Tyscan Ltd., while the functional groups present in each material were analyzed by employing a Nicolet iS10 FT-IR spectrometer (Thermo Fisher Scientific). Furthermore, the elemental chemical forms of each material were identified through examination with a Thermo Scientific ESCALAB 250Xi X-ray photoelectron spectroscope (XPS) from Thermo Fisher Scientific.

2.3.2. Batch Adsorption

A predetermined amount of MRS was carefully measured and transferred to a 150 mL conical flask. Subsequently, an amount of nitrate solution was added to the flask. All batch adsorption experiments were carried out in a water-bath shaker at 180 rpm and at the end of the reaction the mixture was filtered through a nylon membrane with a pore size of 0.45 μm. After filtration, the residual nitrate nitrogen concentration in the supernatant was quantified. Using these data, the nitrate nitrogen removal efficiency (η) and adsorption capacity (q_e) of the MRS were determined. Determination of nitrate concentration in solution followed the protocol outlined in the "Ultraviolet Spectrophotometric Method for the Determination of Nitrate Nitrogen in Water Quality" (HJ/T 346-2007).

$$\eta = \frac{C_0 - C_t}{C_0} \times 100\% \quad (1)$$

$$q_e = \frac{(C_0 - C_t) \times V}{m} \quad (2)$$

where η is the removal rate of nitrate (%); q_e is the adsorption capacity of MRS for nitrate (mg/g); C_0 is the initial nitrate concentration (mg/L); C_t is the residual concentration of nitrate in the solution after adsorption (mg/L); V is the volume of nitrate solution (L); and m is the mass of adsorbent material MRS (g).

In the optimization dosage experiment, varying amounts of MRS ranging from 0.1 g to 0.9 g were precisely measured to correspond to dosages of 2 g/L to 18 g/L, respectively. These measured quantities were then added to individual conical flasks containing 50 mL of a solution with a concentration of 50 mg/L. The flasks were subsequently subjected to oscillation in a water-bath thermostatic oscillator for a duration of 10 min. Following the completion of the reaction, the concentration of nitrate remaining in the filtrate was determined, allowing for the calculation of removal rate and adsorption capacity. Additionally, in the pH testing phase, the initial pH of the nitrate and phosphate solutions was adjusted within the range of 2.0 to 12.0 using solutions of HCl and NaOH.

The kinetic study of MRS was carried out using nitrate nitrogen at an initial concentration of 20 mg/L, 50 mg/L, and 100 mg/L, and the reaction times were set at 1, 5, 10, 20, 30, 45, 60, 90, 120, and 180 min. Adsorption kinetics were carried out by placing 0.4 g of MRS into the solution at 25 °C and 180 rpm in a water bath. In the adsorption isotherm experiments, water baths were maintained at 15, 25, and 35 °C, and 50 mL of NO₃⁻ solution at concentrations of 10–90 mg/L was mixed with 0.1 g of MRS. It was shaken repeatedly at 180 rpm for 10 min.

The expression for the pseudo-first-order kinetic model:

$$\ln(q_e - q_t) = \ln q_e - K_1 t \quad (3)$$

The expression for the pseudo-second-order kinetic model:

$$\frac{t}{q_t} = \frac{1}{K_2 q_e^2} + \frac{t}{q_e} \quad (4)$$

where q_e and q_t represent the amount of nitrate adsorbed by the adsorbent at adsorption equilibrium and at the moment t , respectively (mg/g); t is the adsorption time (min); K_1 is the proposed primary kinetic rate constant (min^{-1}); and K_2 is the proposed secondary kinetic rate constant (min^{-1}).

The expression for the Langmuir isothermal adsorption model:

$$q_e = \frac{K_L Q_{\max} C_e}{1 + K_L C_e} \quad (5)$$

The expression for the Freundlich isothermal adsorption model:

$$q_e = K_f C_e^{1/n} \quad (6)$$

where q_e represents the adsorption capacity of MRS for nitrate nitrogen at adsorption equilibrium (mg/g); C_e represents the concentration of nitrate nitrogen in the solution at equilibrium (mg/L); Q_{\max} represents the theoretical maximum adsorption capacity of MRS for nitrate nitrogen (mg/g); K_L represents the Langmuir adsorption model constant; n and K_f represent the Freundlich adsorption model constants.

2.4. Dynamic Experiment

2.4.1. Dynamic Adsorption and Desorption

The dynamic adsorption setup consisted of a glass fiber reinforced plastic (FRP) column with an inner diameter of 20 mm and a height of 150 mm. Prior to experimentation, quartz sand underwent pretreatment by soaking in 4 mol/L hydrochloric acid for 24 h, followed by five rinses with deionized water and drying. In the experimental procedure, 5 g of pretreated quartz sand was placed at the column base, followed by the addition of a specific mass of modified reed straw (MRS). To immobilize the MRS within the column, 15 g of quartz sand was layered over it to create a level surface. The nitrate solution was introduced at the column base and flowed through the MRS via the use of a peristaltic pump to control the flow rate. Evaluation criteria were established to monitor the dynamic adsorption progress: the penetration point was indicated when the nitrate nitrogen concentration in the effluent reached around 5% of the initial solution concentration.

On the other hand, saturation of MRS adsorption was identified when the effluent's nitrate nitrogen concentration exceeded 95% of the initial solution concentration. Nitrate nitrogen concentrations in the effluent were regularly monitored and plotted for analysis throughout the experiment. Experimental investigations were conducted to study the impact of packing height on adsorption efficiency, with three groups using MRS fillers weighing 1, 2, and 3 g, corresponding to packing heights of 1.1, 2.2, and 3.3 cm, respectively. The outlet nitrate nitrogen concentration was monitored at 5 min intervals. Additionally, the effect of flow rate on adsorption efficiency was studied under variable speed conditions using a nitrate concentration of 50 mg/L, 2 g of MRS filler, and flow rates of 3, 5, and 7 mL/min. Sampling intervals were set at 10, 5, and 5 min, respectively. Finally, the influence of inlet water nitrate nitrogen concentration on adsorption efficiency was explored by adjusting the initial solution's nitrate nitrogen concentration to 20, 50, and 80 mg/L, while maintaining a filling volume of 2 g of MRS and a constant flow rate of 5 mL/min.

Desorption experiments were conducted using the identical column utilized in the adsorption studies, with KCl selected as the desorption solution. Optimal experimental conditions were achieved through careful control of the MRS filling volume, variation in flow rates, and adjustment of the initial solution concentration. These carefully selected

dynamic adsorption and desorption conditions aimed to yield a nitrate nitrogen solution suitable for subsequent resource utilization. The experimental flowchart is shown in Figure 1.



Figure 1. Experimental device diagram.

2.4.2. Dynamic Adsorption Modeling

Thomas Model

The expression is:

$$\ln\left(\frac{C_0}{C_t} - 1\right) = \frac{K_{Th}q_e m}{v} - K_{Th}C_0 t \quad (7)$$

where t (min) is the running time; C_0 (mg/L) is the concentration of nitrate nitrogen in the influent water; C_t (mg/L) is the concentration of nitrate nitrogen in the effluent water at time t ; q_e (mg/g) is the unit adsorption amount of nitrate nitrogen by the MRS after the adsorption equilibrium; m (g) is the mass of the MRS in the packed column; and K_{Th} is the parameter of Thomas' model [25].

Yoon–Nelson Model

The expression for the Yoon–Nelson model is:

$$\frac{C_t}{C_0} = \frac{\exp(K_{YN}t - \tau K_{YN})}{1 + \exp(K_{YN}t - \tau K_{YN})} \quad (8)$$

where τ (min) is the time required for the effluent concentration to be 50% of the influent concentration; C_0 (mg/L) is the nitrate nitrogen concentration in the influent; C_t (mg/L) is the nitrate nitrogen concentration in the effluent at time t ; t (min) is the running time; and K_{YN} (min^{-1}) is the constant of the Yoon–Nelson model [26].

2.5. Capitalizing on Resources

Measurement of fresh weight of corn seedlings: carefully separate the corn seedlings from the soil, gently wipe off any soil adhering to the roots and leaves, and then weigh them using an analytical balance.

Measurement of plant height: measure the length from the base of the corn seedling to its highest point using a ruler.

Determination of chlorophyll content: the chlorophyll content in plant leaves is determined using a spectrophotometric method. Take 0.2 g of fresh plant leaves in a mortar, add a small amount of quartz sand and calcium carbonate powder, grind into a uniform paste after adding 2–3 mL of 95% ethanol, and continue grinding with an additional 10 mL of 95% ethanol until the plant tissue turns white. Filter the homogenate into a 25 mL brown volumetric flask and make up to volume with 95% ethanol. Measure the absorbance of the solution at wavelengths of 663 nm and 645 nm using a UV-Vis spectrophotometer.

Through these experiments, optimal desorption conditions were determined, leading to the development of a resource-efficient desorption solution. Under the optimized conditions, the initial 5 min fraction of the desorption solution was collected and utilized as a nitrate nitrogen nutrient solution for subsequent resource applications.

Because of its short growth cycle and adaptability, corn facilitates the conduct of multiple experiments within a compressed timeframe. Hence, subsequent resource utilization endeavors utilize corn as the primary experimental subject. Resource utilization experiments were performed using maize pot trials, comprising a blank group (BG), high potassium control group (HK), low potassium control group (LK), and a high nitrogen experimental group (HN) and low nitrogen experimental group (LN). Each group was subjected to three replicates, with 5 maize seeds planted in 1000 g of ground soil per experimental group. The control group received varying concentrations of KCl solution, while the experimental group was treated with different concentrations of desorption liquids. Throughout the experiment, equal amounts of deionized water were added to the experimental group daily, and the growth of the plants was monitored and recorded.

3. Results and Discussion

3.1. Physicochemical Characterization of MRS

The morphological characteristics of RS, MRS, and MRS-N were investigated using a scanning electron microscopy (SEM). As depicted in Figure 2a–c, the surface of the RS exhibited a smooth texture, whereas the surfaces of the MRS and MRS-N displayed significant variations [27]. Upon quaternization modification, the cellulose structure of straw was disrupted, resulting in an increase in surface roughness for the MRS and MRS-N. The fibrous structure of the modified material was disrupted, causing the rod-like fibers to break and the arrangement to become disordered. This phenomenon can be attributed to the degradation of cellulose in the reed straw during the modification process [28]. Moreover, this change in morphology facilitates the availability of more attachment sites for the branching quaternary amine groups (Figure 2b,e). Based on the observation from Figure 2f, it can be inferred that the surface of the material is relatively flat, providing initial evidence of successful adsorption of nitrate nitrogen by the material [29].

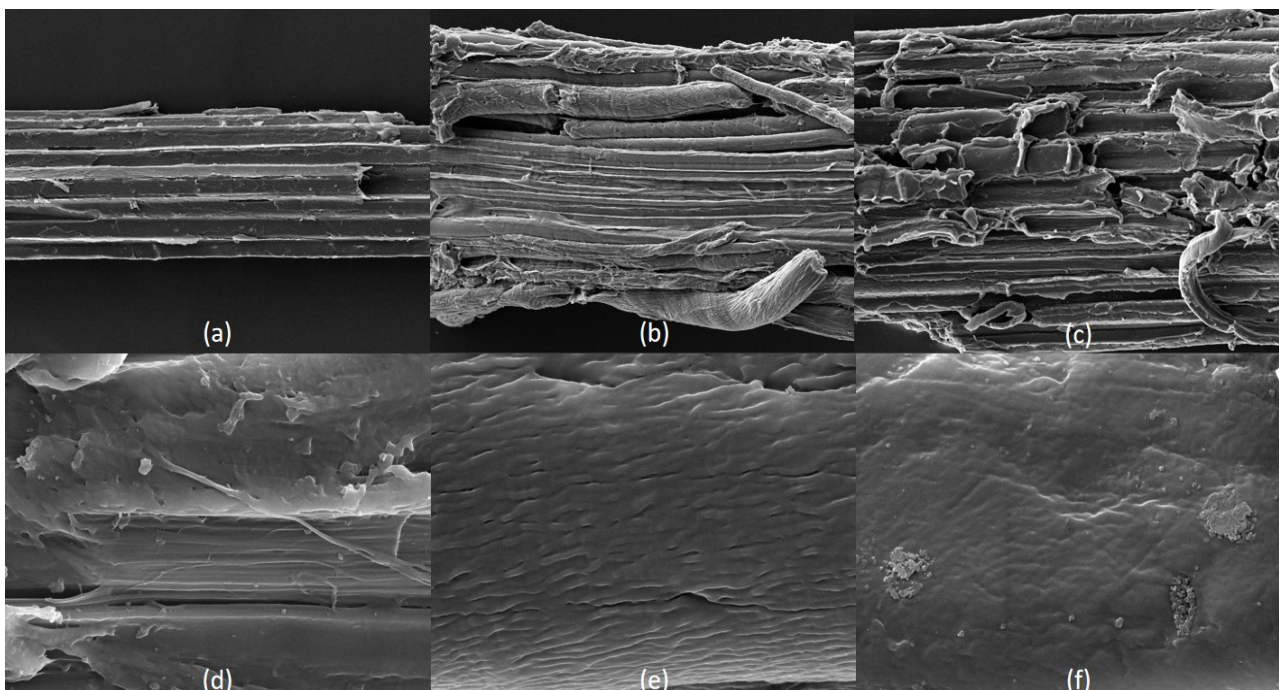


Figure 2. SEM images of (a,d) RS, (b,e) MRS, and (c,f) MRS-N; (a–c) are images after 1k times magnification and (d–f) are images after 50k times magnification.

The FT-IR spectra of RS, MRS, and MRS-N exhibited similar patterns (Figure 3a), suggesting that the fundamental structure of the adsorbents remained largely unchanged after modification [30]. The peaks observed near 3336 and 1029 cm^{-1} were attributed to the vibrations of O-H and C-H in the cellulose. In the case of the MRS, the decreased intensity at 1029 cm^{-1} could be attributed to the cleavage of the C-H band caused by cellulose alkalization [31]. In comparison to the original straw, the appearance of N-H (1731 cm^{-1}) and C-H (1300 cm^{-1}) peaks in the MRS-N indicated the successful grafting of quaternary ammonium groups onto the straw structure, with significantly enhanced intensities of N-H (3336 , 1731 , and 1029 cm^{-1}) peaks [32].

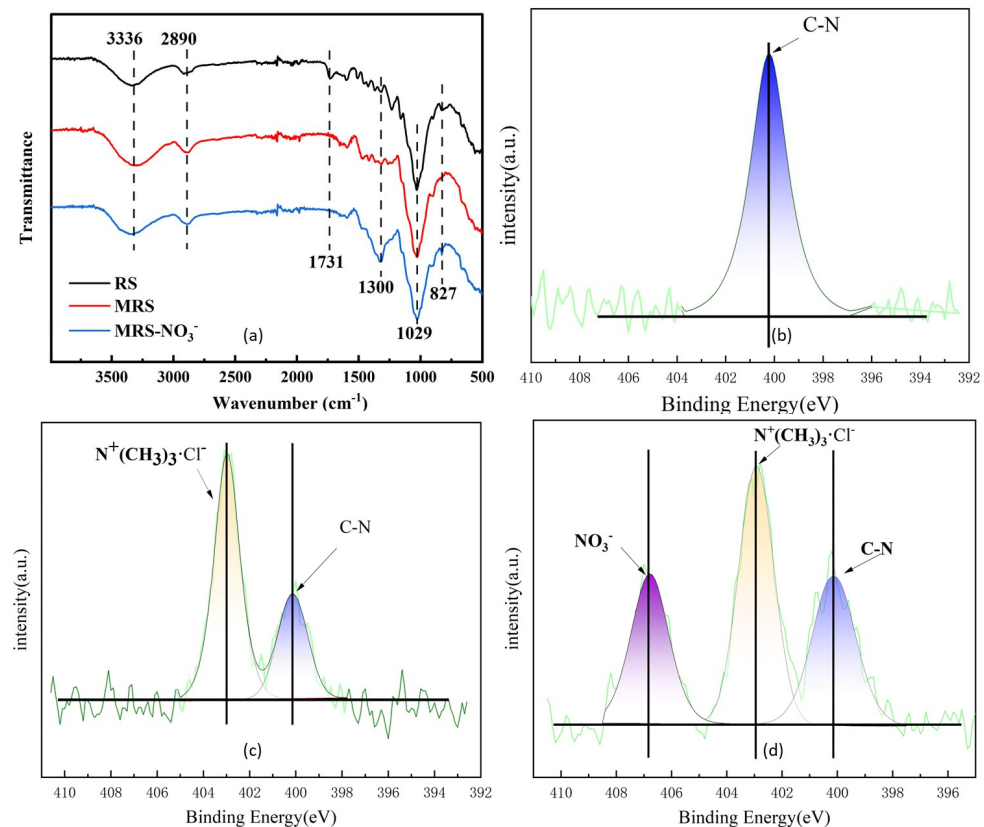


Figure 3. FT-IR of RS, MRS (a), and MRS- NO_3^- and XPS spectra for N 1s in RS (b), MRS (c), and MRS-N (d).

Furthermore, the quaternization reaction resulted in the emergence of a new N 1s XPS peak at 403.1 eV in MRS (Figure 3), corresponding to the $\text{N}^+(\text{CH}_3)_3\text{Cl}^-$ bonding, confirming the successful branching of quaternary amine groups onto the material surface [33,34]. The peak observed at 406.8 eV in the MRS-N was characteristic of NO_3^- , indicating the adsorption of elemental nitrogen in the form of nitrate onto the material surface.

The elemental composition of the materials, including the C, N, O, and Cl, was analyzed through the EDS energy spectra. As depicted in Figure 4, the EDS patterns illustrate distinct characteristics for RS, MRS, and MRS-N.

It is discernible that RS predominantly comprises high concentrations of C and O, while N and Cl exhibit minimal presence, near absence, owing to inherent material properties. In contrast, the MRS exhibits a slight increase in C and N content alongside a minor decrease in O, and a substantial rise in Cl content. This alteration can be attributed primarily to the incorporation of quaternary amine groups and epichlorohydrin during the modification process.

The noticeable augmentation in N and O elements within the MRS-N primarily stems from nitrate adsorption, whereas the Cl content experiences a marked decrease compared to the MRS. This decline is speculated to result from the adsorption of nitrate and chloride

ions during the nitrate adsorption process, possibly facilitated by ion exchange reactions between the chloride and nitrate.

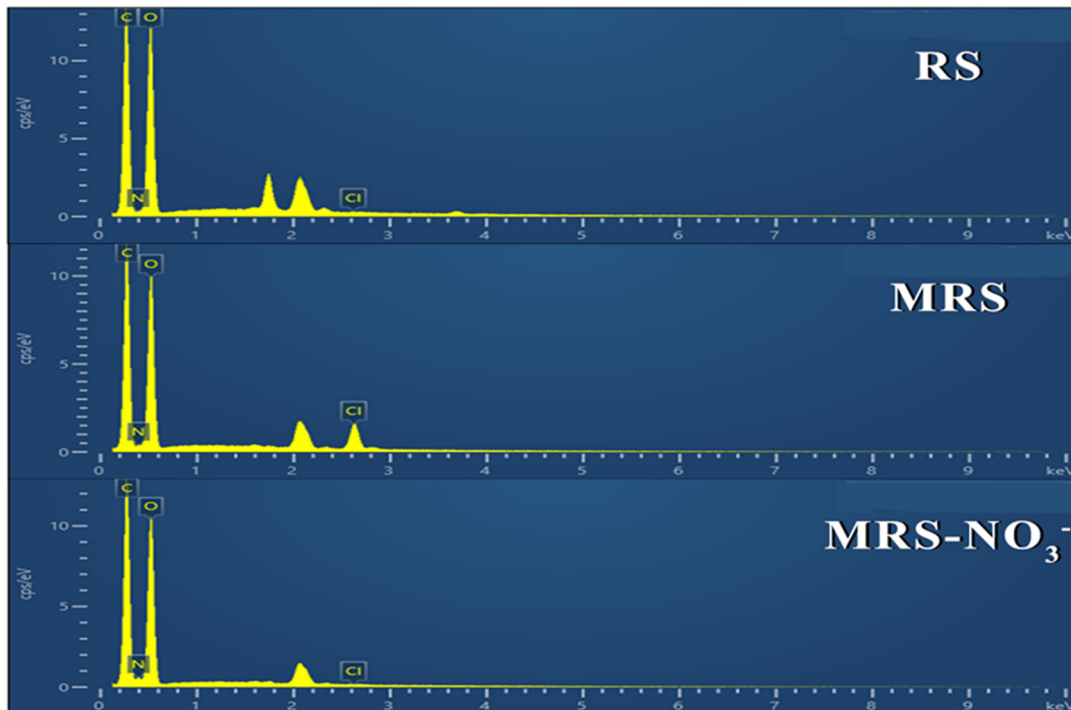


Figure 4. EDS spectrogram of RS, MRS, and MRS-NO₃⁻.

As observed in Table 1, the raw material surface initially exhibits a negative charge with a Zeta potential of -21.2 mV. However, after surface modification, characterized by the introduction of positively charged quaternary amine groups, the Zeta potential significantly shifts to $+40.2$ mV. This transformation primarily arises from the abundance of hydroxyl and carboxyl functional groups, typical of cellulose and hemicellulose, constituting the raw material.

Table 1. Zeta potential value of material.

Material	RS	MRS	MRS-N
Zeta potential/mV	-21.2	$+40.2$	$+9.3$

The attachment of quaternary amine groups onto the material surface introduces positive charges, consequently elevating the material's Zeta potential. Subsequent adsorption of nitrate ions leads to a reduction in the surface Zeta potential. Thus, it can be inferred that the nitrate adsorption mechanism involves electrostatic attraction between the material surface and nitrate ions (Figure 5).

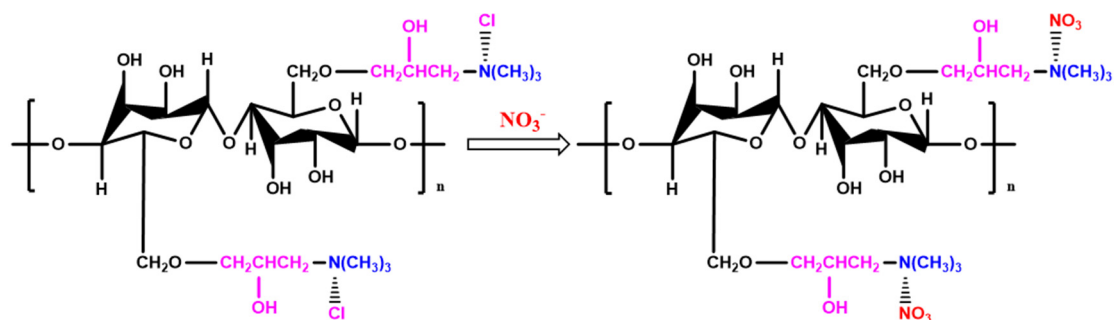


Figure 5. Adsorption process diagram.

3.2. Adsorption Characteristics

As can be seen from Figure 6a, the removal rate of nitrate by the MRS increased with the increase in the dosage, from the initial 25.9% to 86.7%, and with the increase in the dosage, the increase in the removal rate gradually decreased, from the initial 50.8% to 0.4%, while the adsorption capacity gradually decreased with the increase in the dosage, from the initial 6.45 mg/g to 2.71 mg/g. This is mainly due to the fact that with the increase in the dosage, the corresponding nitrate adsorption sites increased, the contact area between the MRS and nitrate increased, and the removal rate increased [35]; however, the nitrate concentration in the solution was limited, and with the decrease in the solution nitrate concentration, the adsorption sites of excess MRS became more and more difficult to combine with the nitrate, which led to the increase in the magnitude of the removal rate and the decrease in the adsorption capacity of the MRS [36]. According to the experimental results, 8 g/L was finally selected as the optimal dosage for this experiment, taking into account the removal rate of nitrate and the utilization rate of MRS. Compared with the unmodified RS, the adsorption capacity of the MRS at the same dosage increased 45 times, from which we can conclude that MRS has good adsorption performance for nitrate nitrogen compared with RS, and the effect of modification is very obvious.

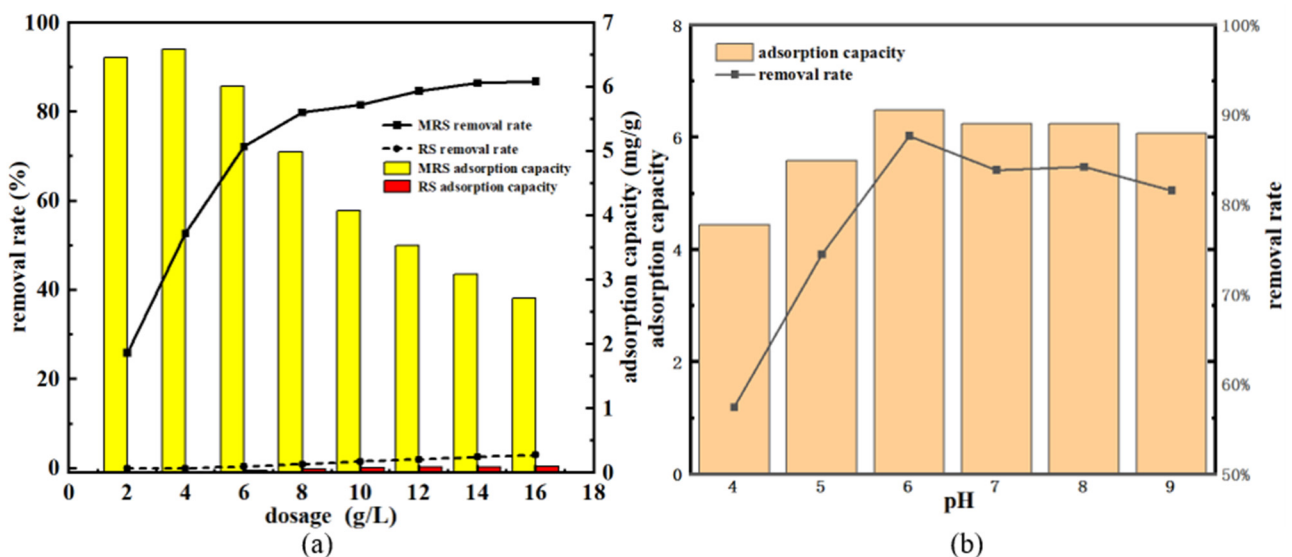


Figure 6. Effect of MRS dosage on adsorption efficiency and adsorption capacity (a) and effect of pH and adsorption efficiency and adsorption capacity of MRS (b).

The impact of solution pH variation (4–9) on nitrate adsorption is depicted in Figure 6b. Within the studied pH range, MRS demonstrates efficient nitrate removal particularly between pH 5 and 9. Under acidic conditions, there is a propensity for pollutant desorption from MRS, diminishing its adsorption capacity. Conversely, in alkaline environments, heightened competition arises between excess OH^- ions and nitrate ions, exacerbating the electrostatic repulsion between anions and MRS, consequently reducing nitrate adsorption efficiency [34].

The interaction mechanism between nitrate nitrogen and MRS was further elucidated by kinetic model fitting (Table 2). The fitting parameters of the kinetic model showed that the R^2 value of the proposed second-order model fit (0.999) was better than that of the proposed first-order model (0.997), and the theoretical adsorption amount of the proposed second-order kinetic was close to the actual equilibrium adsorption amount. The results showed that the adsorption of nitrate after MRS modification was controlled by both physical and chemical adsorption, but the chemical adsorption by ion exchange was dominant.

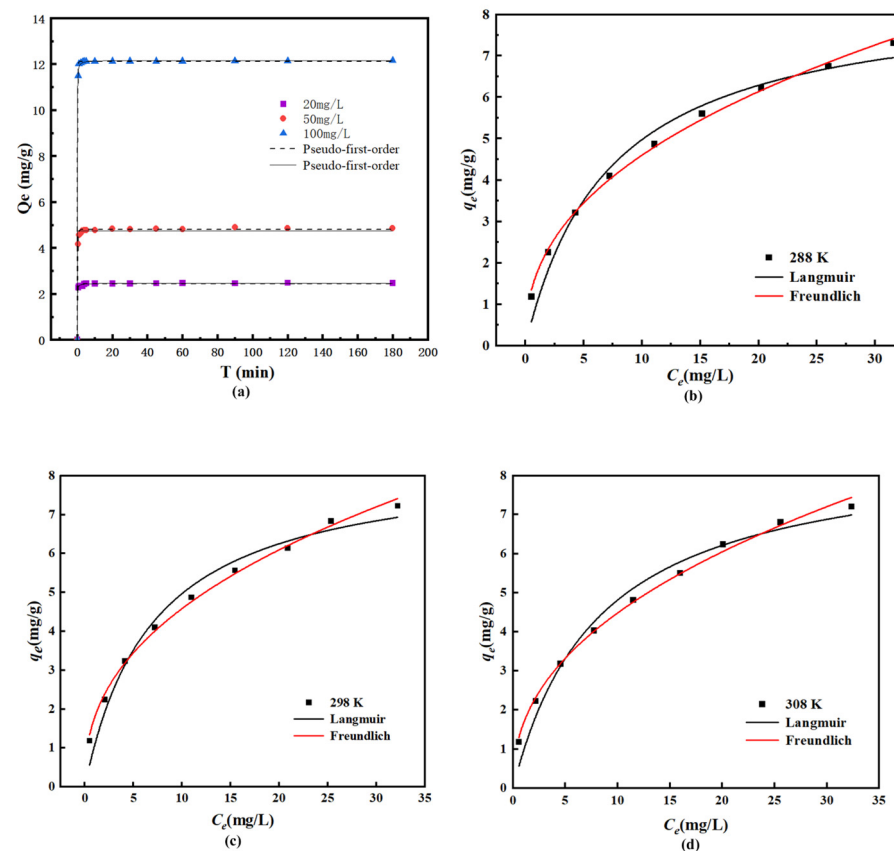
Table 2. Adsorption kinetics data.

	Pseudo-First-Order			Pseudo-Second-Order		
	q_e ($\text{mg}\cdot\text{g}^{-1}$)	K_1 (min^{-1})	R^2	q_e ($\text{mg}\cdot\text{g}^{-1}$)	K_2 ($\text{g}\cdot(\text{mg}\cdot\text{min})^{-1}$)	R^2
20 mg/L	2.44	5.25	0.994	2.45	8.47	0.998
50 mg/L	4.79	3.95	0.997	4.85	2.66	0.999
100 mg/L	12.11	5.93	0.998	12.16	3.35	0.999

The adsorption isotherm effectively delineates the correlation between the number of milligrams adsorbed per gram of MRS and the equilibrium concentration of nitrate (Table 3). Comparatively, the Freundlich model exhibits superior fitting performance when contrasted with the Langmuir model [37]. It is evident that the adsorption of nitrate nitrogen by MRS pertains to multilayer adsorption within a non-uniform phase [38]. Notably, the Freundlich constant 'n' surpasses one across all temperatures, indicating favorable adsorption (Figures 6 and 7).

Table 3. Adsorption isotherm data.

	Langmuir			Freundlich		
	q_{max} ($\text{mg}\cdot\text{g}^{-1}$)	K_L	R^2	n	K_F	R^2
288 (k)	8.54	0.139	0.976	2.29	1.69	0.998
298 (k)	8.43	0.143	0.976	2.43	1.78	0.996
308 (k)	8.76	0.122	0.976	2.31	1.66	0.997

**Figure 7.** Adsorption kinetics (a) and adsorption isotherms (b–d) of nitrate on MRS.

The paper evaluated the adsorption capacity and efficiency of various adsorbents, as shown in Table 4. The use of trimethylamine in this study led to significantly improved

adsorption performance compared to reed modification with ethylenediamine and diethylamine [39]. Additionally, the modification process outlined here was simple and yielded better adsorption results compared to biochar-modified adsorbents [40,41]. Moreover, this study introduced a new method for resource utilization, thus establishing a model for resourceful utilization in the treatment process.

Table 4. Comparison of adsorption performance of different adsorbents on nitrate nitrogen.

Absorbent	Maximum Adsorption Capacity (mg/g)	Removal Rate
CPB-modified zeolite [42]	4.70	/
Modified cattail biochar [39]	5.56	56%
Modified reed [40]	4.24	47%
Iron-modified biochar [41]	4.49	/
present study	8.54	80%

3.3. Dynamic Adsorption and Desorption of MRS

3.3.1. Dynamic Adsorption Experiment

The study examined the impact of packing height, solution flow rate, and initial concentration on the dynamic adsorption effects of MRS. Three experimental groups with packing heights of 1.1, 2.2, and 3.3 cm were tested at a flow rate of 5 mL/min and a nitrate nitrogen concentration of 50 mg/L. The results showed (Figure 8a) that increasing packing height led to more ion exchange sites, extending mass transfer zones and increasing penetration and saturation times [43].

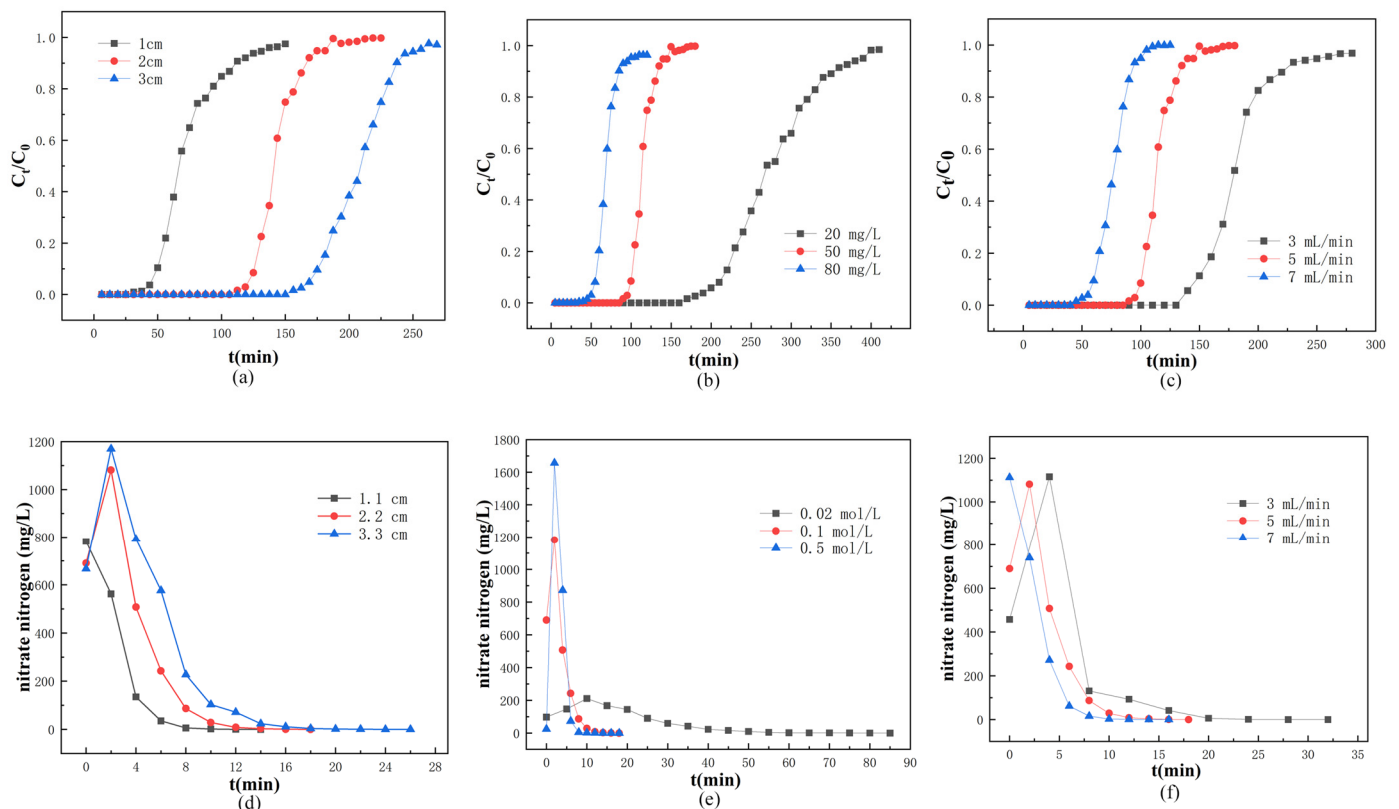


Figure 8. Graphs (a–c) show the effect of packing height, flow rate, and initial concentration on dynamic adsorption, respectively, and (d–f) show the effect of packing height, solution flow rate, and desorption reagent concentration on the dynamic desorption effect, respectively.

In another experiment varying solution flow rates (3, 5, and 7 mL/min) at a fixed packing height of 2.2 cm and concentration of 50 mg/L, higher flow rates shortened

permeation and saturation times but reduced nitrate adsorption due to a shorter mass transfer distance (Figure 8b). Consequently, total and unit adsorption amounts decreased, limiting contact time between the solution and the material [44].

The investigation also explored the influence of initial solution concentrations (20, 50, and 80 mg/g) on dynamic adsorption (Figure 8c). Higher initial concentrations advanced penetration and saturation points, leading to increased adsorption amounts attributed to accelerated reaction rates and improved contact opportunities between nitrate nitrogen and MRS sites. This heightened concentration gradient boosted the material's adsorption capacity significantly.

3.3.2. Dynamic Model Fitting

Through dynamic adsorption experiments, the impact of modified reed straw (MRS) on the removal of nitrate nitrogen under varied conditions was elucidated, employing dynamic adsorption models to interpret the results and unveil the adsorption mechanisms involved.

Thomas Model

The Thomas model, well-suited for Langmuir adsorption–desorption phenomena, internal/external diffusion processes, and secondary reversible reactions, characterizes adsorption under fixed-bed advection flow. By employing Langmuir adsorption isotherms and secondary reversible reactions, the dynamic adsorption behavior of MRS was analyzed.

Simulation parameters are outlined in Table 5, demonstrating satisfactory fitting of the Thomas dynamic model across different packing heights and initial flow rates, with linear correlation coefficients (R) consistently surpassing 0.9000. This underscores the efficacy of the Thomas model in delineating the dynamic adsorption of nitrate nitrogen by MRS, where both internal and external diffusion contribute without rate-limiting steps. Notably, as flow velocity escalates, the Thomas model parameter (K_{th}) increases, indicating heightened flow turbulence. However, excessively high flow rates can impede material utilization, necessitating the selection of optimal flow rates to enhance reaction rates while ensuring material efficacy.

Table 5. Thomas model parameters.

Column Height (cm)	Initial Flow Rate (mL/min)	Initial Concentration (mg/L)	K_{th} (mL/min/mg)	q_e (mg/g)	R^2
1.1	5	50	1.35	14.37	0.932
2.2	5	50	2.57	14.39	0.949
3.3	5	50	1.66	13.81	0.993
2.2	3	50	1.02	13.76	0.939
2.2	7	50	2.66	13.34	0.996
2.2	5	20	1.47	13.92	0.981
2.2	5	80	1.50	13.92	0.945

Yoon–Nelson Model

The Yoon–Nelson model forecasts penetration time except at 50% adsorption, offering valuable insights into dynamic adsorption processes. Table 6 showcases the favorable fitting outcomes of the Yoon–Nelson model, with linear correlation coefficients consistently exceeding 0.9000. This underscores the model's efficacy in capturing the dynamic adsorption dynamics of nitrate nitrogen by MRS. Notably, as flow rates rise, the Yoon–Nelson model constant (K_{YN}) increases, inversely affecting τ , thus, shortening penetration and saturation times [45].

Table 6. Yoon–Nelson model parameters.

Column Height (cm)	Initial Flow Rate (mL/min)	Initial Concentration (mg/L)	K_{YN} (min^{-1})	T (min)	R^2
1.1	5	50	0.0673	57.49	0.932
2.2	5	50	0.1284	115.09	0.949
3.3	5	50	0.0829	165.78	0.993
2.2	3	50	0.0508	183.45	0.939
2.2	7	50	0.1328	76.24	0.996
2.2	5	20	0.0293	278.37	0.981
2.2	5	80	0.1198	69.61	0.945

3.3.3. Desorption Experiment

The study identified pivotal factors affecting dynamic adsorption efficiency, including packing height, solution flow rate, and desorption reagent concentration. Packing height significantly influenced total adsorption column capacity, as demonstrated in Figure 8d, which showed increased nitrate desorption with expanded mass transfer distance at heightened packing heights. Desorption experiments revealed the impact of solution concentration on ion-exchange reactions, wherein higher concentrations led to elevated maximum nitrate concentrations in effluent, as depicted in Figure 8e. Additionally, increasing flow rates reduced contact time between the desorbing solution and MRS, requiring greater solution volumes for complete desorption, as shown in Figure 8f. Despite this, maximum nitrate nitrogen concentrations remained relatively stable across varied flow rates, indicating limited impact on desorption efficiency. Overall, these findings highlight the critical role of packing height, solution flow rate, and desorption reagent concentration in influencing dynamic adsorption processes.

3.4. Nitrate Nitrogen Resource Utilization

3.4.1. Desorbent Resource Utilization

In the desorption experiment, the desorption solution obtained from the initial five fractions was identified as the nutrient solution due to its notably high relative nitrate nitrogen content, averaging 842.5 mg/g. Furthermore, the enrichment multiplier of this nutrient solution reached 16.8 times that of the initial solution. By applying this nutrient solution to the soil, the growth of experimental subjects was effectively stimulated. The utilization of MRS enables a cyclic adsorption and desorption process, facilitating the continuous conversion of original sewage pollutants into fertilizer in the form of nitrate. This process significantly contributes to promoting crop growth. Therefore, it can be concluded that the resourceful utilization of desorption solution represents a pivotal approach towards maximizing the utilization of nitrate nitrogen resources in sewage treatment.

3.4.2. Effects of Desorbing Solutions on Plants

The experimental groups were categorized into five distinct groups: the blank group (BG), the high-potassium control group (HK), the low-potassium control group (LK), alongside the high-nitrogen experimental group (HN), and the low-nitrogen experimental group (LN).

Following the application of the nutrient solution, the impact on plant growth is visually depicted in Figure 9a. Through daily measurements of plant column heights, the average plant heights were ranked as follows: $HN > LN > HK > LK > BG$. A notable enhancement in plant height was observed in the LN and HN groups, with increases of 18.7% and 28.5%, respectively, compared to the blank group. This enhancement can be attributed to the promotion effect of both KCl solution and desorption solution on corn growth, primarily due to their potassium content, which plays a crucial role in plant development. The superior plant height in the experimental group compared to the control group can be attributed to the provision of nitrogen for plant growth by the nitrate

nitrogen in the desorption solution, with higher concentrations leading to more pronounced growth promotion.

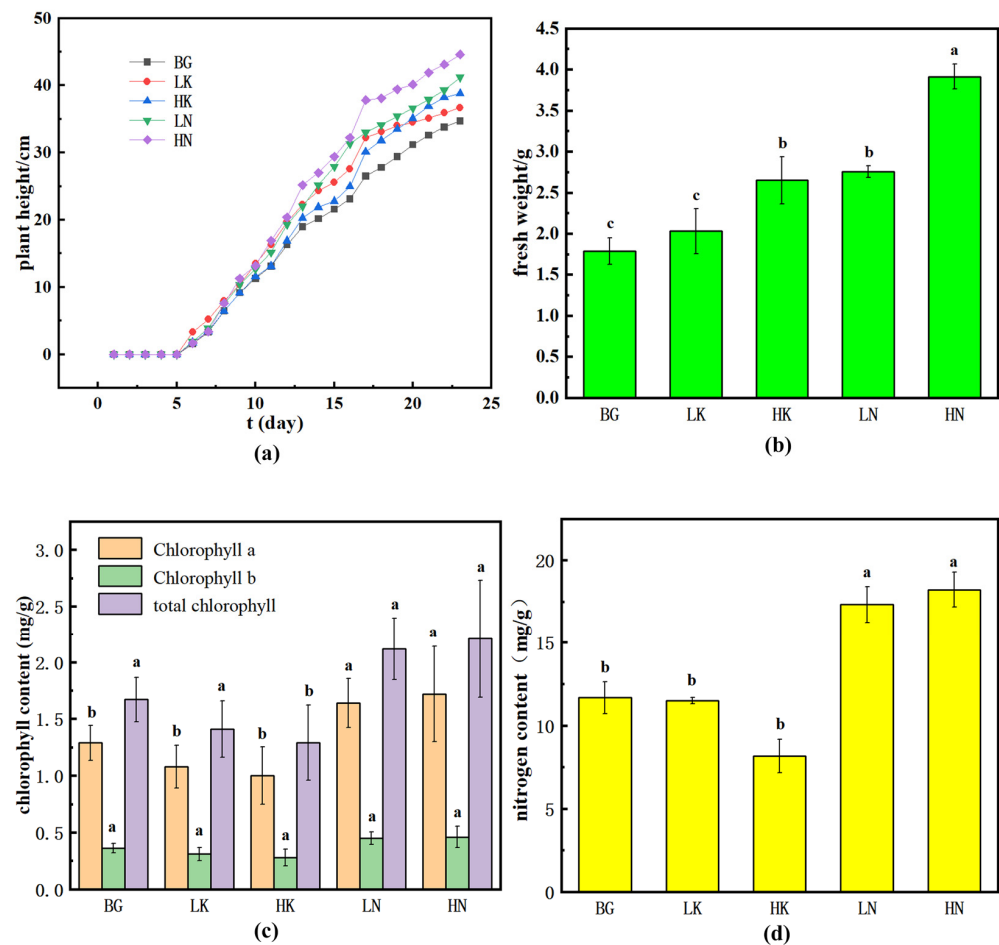


Figure 9. (a) Effect of desorption solution on plant height and growth; (b) effect of desorption solution on plant fresh weight; (c) effect of desorption solution on plant chlorophyll content; and (d) effect of desorption solution on plant nitrogen content. (The variability between charts a, b, and c has been examined and the results show consistency within the same letter grouping and a great deal of variability between different letter groups).

Significantly higher fresh weights were recorded in both control and experimental groups compared to BG, with LK and HK pairs exhibiting increases of 5.3% and 26.9%, respectively, indicating the growth-promoting effect of the potassium from the KCl solution (Figure 9b). In contrast, LN and HN groups displayed remarkable fresh weight increments of 43.2% and 96.4%, respectively, compared to BG, highlighting the combined promotion of nitrogen and potassium from the desorption solution, with nitrogen playing a primary role in fresh weight enhancement. The robustness of plants in the experimental group, observed through both height and weight measurements, supports the feasibility of using desorbed liquid as a nitrogen supplement to enhance plant growth.

Furthermore, the chlorophyll content of plants in the experimental group surpassed that of other groups by 26.9% and 32.3% compared to BG, indicating an increase resulting from the nitrogen application in the nutrient solution (Figure 9c). The chlorophyll content of plants in the nitrogen application group surpassed that of other groups, indicating an elevation in chlorophyll levels due to the nitrogen present in the applied nutrient solution. Specifically, within this group, the chlorophyll content in the high nitrogen (HN) subgroup exceeded that of the low nitrogen (LN) subgroup, suggesting a positive correlation between nitrogen application levels and chlorophyll enhancement in plants.

This finding aligns with prior research by other scholars [46]. Conversely, plants in the potassium group exhibited lower chlorophyll content compared to the blank group (BG), with high potassium (HK) displaying inferior levels compared to low potassium (LK). This disparity can be attributed to nitrogen's role as a constituent element of chlorophyll [47]. Since no additional nitrogen was applied to any of the three groups, and considering the plant height and fresh weight sequence (HK > LK > nitrogen application group), the nitrogen content per unit mass of plants followed the pattern HK < LK < BG, thereby constraining chlorophyll production. This underscores the potential of utilizing desorbed solutions as nutrient supplements to meet the nitrogen requirements crucial for plant growth and development, consequently augmenting chlorophyll levels and facilitating overall plant growth and development.

Analysis of nitrogen content revealed a significant increase in the experimental group, particularly in the LN and HN groups, with levels 47.9% and 55.6% higher than BG (Figure 9d), respectively. This phenomenon primarily stems from the application of a nitrogen-containing nutrient solution to the nitrogen application group, leading to nitrogen absorption by the plants and consequently elevating their nitrogen content. Notably, the nitrogen content in the potassium group was inferior to that in the BG, while HK exhibited lower nitrogen content compared to LK. This disparity can be attributed to the superior plant height and fresh weight observed in the nitrogen application group, surpassing those of the BG, with HN demonstrating further enhancement compared to LN. Despite the absence of additional nitrogen fertilizers, the total nitrogen content in the soil remained consistent, resulting in a lower nitrogen content per unit mass in plants exhibiting robust growth. These observations suggest that the nitrogen present in the desorption solution was effectively absorbed and utilized by the plants, thereby endorsing the feasibility of utilizing desorption solutions as a nitrogen supplement for plant growth.

4. Conclusions

A biomass adsorbent with high nitrate nitrogen adsorption capacity was successfully synthesized through a quaternization reaction, introducing quaternary amine groups into the internal structure of straw and creating favorable adsorption sites for nitrate nitrogen. Characterization via SEM, XPS, and FT-IR techniques confirmed the successful modification of the adsorbent.

The findings from dynamic adsorption and desorption experiments revealed intriguing insights. The penetration time of the packed column during dynamic adsorption was observed to increase with column height growth, while decreasing with higher flow rates and initial concentrations. In dynamic desorption, the concentration of nitrate nitrogen in the desorbed solution was primarily influenced by column height and solution concentration, with a lesser impact from flow rate variations. The enrichment of nitrate nitrogen through dynamic desorption lays a solid foundation for resource utilization, leading to the development of a nutrient solution with enhanced nitrate nitrogen content suitable for application as liquid fertilizer to enrich soil fertility.

Moreover, the recyclable sorbent (MRS) displayed commendable reusability, stability, and superior phosphate removal efficiency. These qualities position MRS as a promising candidate for diverse water and wastewater treatment applications, including addressing issues like water body eutrophication, agricultural wastewater treatment, and domestic sewage purification.

Author Contributions: Conceptualization, H.Z., Z.Y., J.T. and C.L.; methodology, H.Z., C.L. and J.T.; software, H.Z. and Z.Y.; validation, H.Z., Z.Y., J.T. and C.L.; formal analysis, H.Z. and Z.Y.; investigation, C.L., J.T. and Z.Y.; resources, J.T. and C.L.; data curation, H.Z.; writing—original draft, H.Z.; writing—review & editing, Z.Q.; visualization, C.L.; project administration, Z.Q. All authors have read and agreed to the published version of the manuscript.

Funding: Financial support for this research was provided by the Key R&D Project of Hebei Province (21373601D); Supported by the Collaborative Innovation Center for Baiyangdian Basin Ecological Protection and Beijing-Tianjin-Hebei Sustainable Development.

Institutional Review Board Statement: Not applicable.

Informed Consent Statement: Not applicable.

Data Availability Statement: Data is contained within the article.

Conflicts of Interest: The authors declare no conflicts of interest.

References

1. Ma, L.; Hu, L.; Feng, X.; Wang, S. Nitrate and Nitrite in Health and Disease. *Aging Dis.* **2018**, *9*, 938. [\[CrossRef\]](#)
2. Ackerman, D.; Millet, D.B.; Chen, X. Global Estimates of Inorganic Nitrogen Deposition across Four Decades. *Glob. Biogeochem. Cycles* **2019**, *33*, 100–107. [\[CrossRef\]](#)
3. Liu, J.; Su, J.; Ali, A.; Wang, Z.; Chen, C.; Xu, L. Role of Porous Polymer Carriers and Iron-Carbon Bioreactor Combined Micro-Electrolysis and Biological Denitrification in Efficient Removal of Nitrate from Wastewater under Low Carbon to Nitrogen Ratio. *Bioresour. Technol.* **2021**, *321*, 124447. [\[CrossRef\]](#)
4. Li, R.; Feng, C.; Hu, W.; Xi, B.; Chen, N.; Zhao, B.; Liu, Y.; Hao, C.; Pu, J. Woodchip-Sulfur Based Heterotrophic and Autotrophic Denitrification (WSHAD) Process for Nitrate Contaminated Water Remediation. *Water Res.* **2016**, *89*, 171–179. [\[CrossRef\]](#) [\[PubMed\]](#)
5. Priya, E.; Kumar, S.; Verma, C.; Sarkar, S.; Maji, P.K. A Comprehensive Review on Technological Advances of Adsorption for Removing Nitrate and Phosphate from Waste Water. *J. Water Process Eng.* **2022**, *49*, 103159. [\[CrossRef\]](#)
6. Li, M.; Gu, H.; Lam, S.S.; Sonne, C.; Peng, W. Deposition-Mediated Phytoremediation of Nitrogen Oxide Emissions. *Environ. Pollut.* **2022**, *308*, 119706. [\[CrossRef\]](#) [\[PubMed\]](#)
7. Zhan, Q.; Stratmann, C.N.; van der Geest, H.G.; Veraart, A.J.; Brenzinger, K.; Lüring, M.; de Senerpont Domis, L.N. Effectiveness of Phosphorus Control under Extreme Heatwaves: Implications for Sediment Nutrient Releases and Greenhouse Gas Emissions. *Biogeochemistry* **2021**, *156*, 421–436. [\[CrossRef\]](#)
8. Sun, J.; Liu, L.; Yang, F. Electro-Enhanced Chlorine-Mediated Ammonium Nitrogen Removal Triggered by an Optimized Catalytic Anode for Sustainable Saline Wastewater Treatment. *Sci. Total Environ.* **2021**, *776*, 146035. [\[CrossRef\]](#) [\[PubMed\]](#)
9. Abbach, W.; Laghlimi, C.; Isaad, J. Amine-Grafted Pomegranate Peels for the Simultaneous Removal of Nitrate and Phosphate Anions from Wastewater. *Sustainability* **2023**, *15*, 13991. [\[CrossRef\]](#)
10. Schindler, D.W.; Carpenter, S.R.; Chapra, S.C.; Hecky, R.E.; Orihel, D.M. Reducing Phosphorus to Curb Lake Eutrophication Is a Success. *Environ. Sci. Technol.* **2016**, *50*, 8923–8929. [\[CrossRef\]](#)
11. Dai, Y.; Wang, W.; Lu, L.; Yan, L.; Yu, D. Utilization of Biochar for the Removal of Nitrogen and Phosphorus. *J. Clean. Prod.* **2020**, *257*, 120573. [\[CrossRef\]](#)
12. Du, R.; Peng, Y.; Ji, J.; Shi, L.; Gao, R.; Li, X. Partial Denitrification Providing Nitrite: Opportunities of Extending Application for Anammox. *Environ. Int.* **2019**, *131*, 105001. [\[CrossRef\]](#) [\[PubMed\]](#)
13. Fernandez, M.E.; Nunell, G.V.; Bonelli, P.R.; Cukierman, A.L. Activated Carbon Developed from Orange Peels: Batch and Dynamic Competitive Adsorption of Basic Dyes. *Ind. Crops Prod.* **2014**, *62*, 437–445. [\[CrossRef\]](#)
14. Shi, Q.; Zhang, S.; Xie, M.; Christodoulatos, C.; Meng, X. Competitive Adsorption of Nitrate, Phosphate, and Sulfate on Amine-Modified Wheat Straw: In-Situ Infrared Spectroscopic and Density Functional Theory Study. *Environ. Res.* **2022**, *215*, 114368. [\[CrossRef\]](#) [\[PubMed\]](#)
15. Mei, Y.; Xu, J.; Zhang, Y.; Li, B.; Fan, S.; Xu, H. Effect of Fe–N Modification on the Properties of Biochars and Their Adsorption Behavior on Tetracycline Removal from Aqueous Solution. *Bioresour. Technol.* **2021**, *325*, 124732. [\[CrossRef\]](#)
16. Liu, Y.; Zhang, X.; Wang, J. A Critical Review of Various Adsorbents for Selective Removal of Nitrate from Water: Structure, Performance and Mechanism. *Chemosphere* **2022**, *291*, 132728. [\[CrossRef\]](#)
17. Hu, W.; Wang, L.; Zhu, K.; Wu, F.; Qiao, H.; Li, Y. Facile Copolymerization Synthesis of Vinylimidazole/Dibromodecane/Vinylpyridine Polymer with High Capacity for Selective Adsorption of Nitrate from Water. *J. Water Process Eng.* **2022**, *49*, 103052. [\[CrossRef\]](#)
18. Rezanian, S.; Park, J.; Rupani, P.F.; Darajeh, N.; Xu, X.; Shahrokhishahraki, R. Phytoremediation Potential and Control of Phragmites Australis as a Green Phytomass: An Overview. *Environ. Sci. Pollut. Res.* **2019**, *26*, 7428–7441. [\[CrossRef\]](#) [\[PubMed\]](#)
19. Stipniece-Jekimova, A.A.; Teirumnieka, E.; Blumberga, D. When Reed Application Is Sustainable. *Environ. Clim. Technol.* **2022**, *26*, 697–707. [\[CrossRef\]](#)
20. Wang, J.; Yan, L.; Ren, Q.; Fan, L.; Zhang, F.; Shi, Z. Facile Hydrothermal Treatment Route of Reed Straw-Derived Hard Carbon for High Performance Sodium Ion Battery. *Electrochim. Acta* **2018**, *291*, 188–196. [\[CrossRef\]](#)
21. Qi, K.; Song, M.; Xie, X.; Wen, Y.; Wang, Z.; Wei, B.; Wang, Z. CQDs/Biochar from Reed Straw Modified Z-Scheme MgIn₂S₄/BiOCl with Enhanced Visible-Light Photocatalytic Performance for Carbamazepine Degradation in Water. *Chemosphere* **2022**, *287*, 132192. [\[CrossRef\]](#) [\[PubMed\]](#)
22. Liu, N.; Wu, C.; Lyu, G.; Li, M. Efficient Adsorptive Removal of Short-Chain Perfluoroalkyl Acids Using Reed Straw-Derived Biochar (RESCA). *Sci. Total Environ.* **2021**, *798*, 149191. [\[CrossRef\]](#) [\[PubMed\]](#)

23. Liu, G.; Zheng, H.; Zhai, X.; Wang, Z. Characteristics and Mechanisms of Microcystin-LR Adsorption by Giant Reed-Derived Biochars: Role of Minerals, Pores, and Functional Groups. *J. Clean. Prod.* **2018**, *176*, 463–473. [[CrossRef](#)]
24. Song, R.; Yang, S.; Xu, H.; Wang, Z.; Chen, Y.; Wang, Y. Adsorption Behavior and Mechanism for the Uptake of Fluoride Ions by Reed Residues. *Int. J. Environ. Res. Public Health* **2018**, *15*, 101. [[CrossRef](#)] [[PubMed](#)]
25. Amiri, M.J.; Khozaei, M.; Gil, A. Modification of the Thomas Model for Predicting Unsymmetrical Breakthrough Curves Using an Adaptive Neural-Based Fuzzy Inference System. *J. Water Health* **2019**, *17*, 25–36. [[CrossRef](#)] [[PubMed](#)]
26. Li, H.; He, J.; Chen, K.; Shi, Z.; Li, M.; Guo, P.; Wu, L. Dynamic Adsorption of Sulfamethoxazole from Aqueous Solution by Lignite Activated Coke. *Materials* **2020**, *13*, 1785. [[CrossRef](#)] [[PubMed](#)]
27. Xu, X.; Gao, B.; Yue, Q.; Li, Q.; Wang, Y. Nitrate Adsorption by Multiple Biomaterial Based Resins: Application of Pilot-Scale and Lab-Scale Products. *Chem. Eng. J.* **2013**, *234*, 397–405. [[CrossRef](#)]
28. Namasivayam, C.; Sureshkumar, M.V. Removal of Chromium(VI) from Water and Wastewater Using Surfactant Modified Coconut Coir Pith as a Biosorbent. *Bioresour. Technol.* **2008**, *99*, 2218–2225. [[CrossRef](#)] [[PubMed](#)]
29. Sun, X.; Yang, L.; Li, Q.; Zhao, J.; Li, X.; Wang, X.; Liu, H. Amino-Functionalized Magnetic Cellulose Nanocomposite as Adsorbent for Removal of Cr(VI): Synthesis and Adsorption Studies. *Chem. Eng. J.* **2014**, *241*, 175–183. [[CrossRef](#)]
30. Ren, Z.; Xu, X.; Wang, X.; Gao, B.; Yue, Q.; Song, W.; Zhang, L.; Wang, H. FTIR, Raman, and XPS Analysis during Phosphate, Nitrate and Cr(VI) Removal by Amine Cross-Linking Biosorbent. *J. Colloid Interface Sci.* **2016**, *468*, 313–323. [[CrossRef](#)]
31. Oliveira, C.S.; Airoidi, C. Pyridine Derivative Covalently Bonded on Chitosan Pendant Chains for Textile Dye Removal. *Carbohydr. Polym.* **2014**, *102*, 38–46. [[CrossRef](#)] [[PubMed](#)]
32. Oyervides-Muñoz, E.; Pollet, E.; Ulrich, G.; de Jesús Sosa-Santillán, G.; Avérous, L. Original Method for Synthesis of Chitosan-Based Antimicrobial Agent by Quaternary Ammonium Grafting. *Carbohydr. Polym.* **2017**, *157*, 1922–1932. [[CrossRef](#)] [[PubMed](#)]
33. Song, W. Adsorption of Nitrate from Aqueous Solution by Magnetic Amine-Crosslinked Biopolymer Based Corn Stalk and Its Chemical Regeneration Property. *J. Hazard. Mater.* **2016**, *304*, 280–290. [[CrossRef](#)] [[PubMed](#)]
34. Zhang, L.; Meng, F.; Song, W.; Ren, X.; Wang, J.; Cai, X.; Li, X.; Li, Y.; Yan, L. Enhanced Selective Removal of Phosphate in the Presence of High-Strength Nitrate Using Straw-Based Anion Imprinted Biosorbent. *J. Environ. Chem. Eng.* **2022**, *10*, 108060. [[CrossRef](#)]
35. Wang, X.; Lü, S.; Gao, C.; Feng, C.; Xu, X.; Bai, X.; Gao, N.; Yang, J.; Liu, M.; Wu, L. Recovery of Ammonium and Phosphate from Wastewater by Wheat Straw-Based Amphoteric Adsorbent and Reusing as a Multifunctional Slow-Release Compound Fertilizer. *ACS Sustain. Chem. Eng.* **2016**, *4*, 2068–2079. [[CrossRef](#)]
36. Katal, R.; Baei, M.S.; Rahmati, H.T.; Esfandian, H. Kinetic, Isotherm and Thermodynamic Study of Nitrate Adsorption from Aqueous Solution Using Modified Rice Husk. *J. Ind. Eng. Chem.* **2012**, *18*, 295–302. [[CrossRef](#)]
37. Zhang, H.; Li, C.; Chen, X.; Fu, H.; Chen, Y.; Ning, S.; Fujita, T.; Wei, Y.; Wang, X. Layered Ammonium Vanadate Nanobelt as Efficient Adsorbents for Removal of Sr²⁺ and Cs⁺ from Contaminated Water. *J. Colloid Interface Sci.* **2022**, *615*, 110–123. [[CrossRef](#)] [[PubMed](#)]
38. Wang, T.; Wang, J.; Wu, C.; Zhao, M.; Ge, T. Disturbance-Rejection Control for the Hover and Transition Modes of a Negative-Buoyancy Quad Tilt-Rotor Autonomous Underwater Vehicle. *Appl. Sci.* **2018**, *8*, 2459. [[CrossRef](#)]
39. Wang, B.; Qu, Q.; Lu, Z.; Li, F. Adsorption Effect of Modified Aquatic Plants on Nitrate and Phosphate in Water. *Ecol. Sci.* **2017**, *36*, 108–113. [[CrossRef](#)]
40. Wang, B.; Ye, C.; Li, F.; Qu, Q.; Chen, X. Study on Adsorption Regularity of Nitrate Nitrogen by Aquatic Plant-made Biochar. *Chin. J. Environ. Sci.* **2017**, *37*, 116–122.
41. He, K.; Jiang, Y.; Zhou, L.; Han, M.; Jin, J. Experimental Study on Adsorption of Nitrogen and Phosphorus in Initial Rainfall by Iron-modified Biochar. *Environ. Sci. Technol.* **2022**, *45*, 78–86. [[CrossRef](#)]
42. Du, Q.; Chen, Y. Research Progress on Modified Zeolite Treatment of Nitrate in Water. *Appl. Chem. Ind.* **2023**, *52*, 1830–1835. [[CrossRef](#)]
43. Ahmad, A.A.; Hameed, B.H. Fixed-Bed Adsorption of Reactive Azo Dye onto Granular Activated Carbon Prepared from Waste. *J. Hazard. Mater.* **2010**, *175*, 298–303. [[CrossRef](#)]
44. Kundu, S.; Gupta, A.K. Analysis and Modeling of Fixed Bed Column Operations on as(V) Removal by Adsorption onto Iron Oxide-Coated Cement (IOCC). *J. Colloid Interface Sci.* **2005**, *290*, 52–60. [[CrossRef](#)]
45. Martín-Lara, M.A.; Blázquez, G.; Trujillo, M.C.; Pérez, A.; Calero, M. New Treatment of Real Electroplating Wastewater Containing Heavy Metal Ions by Adsorption onto Olive Stone. *J. Clean. Prod.* **2014**, *81*, 120–129. [[CrossRef](#)]
46. Silva, M.A.G.D.; Muniz, A.S.; Mannigel, A.R.; Porto, S.M.A.; Marchetti, M.E.; Nolla, A.; Grannemann, I. Monitoring and Evaluation of Need for Nitrogen Fertilizer Topdressing for Maize Leaf Chlorophyll Readings and the Relationship with Grain Yield. *Braz. Arch. Biol. Technol.* **2011**, *54*, 665–674. [[CrossRef](#)]
47. Wierzbowska, J.; Wierzbowska, J.; Żuk-Gołaszewska, K. The Impact of Nitrogen Fertilization and Rhizobium Inoculation on the Yield and Quality of *Trigonella foenum-graecum* L. *J. Elem.* **2014**, *19*, 1109–1117. [[CrossRef](#)]

Disclaimer/Publisher's Note: The statements, opinions and data contained in all publications are solely those of the individual author(s) and contributor(s) and not of MDPI and/or the editor(s). MDPI and/or the editor(s) disclaim responsibility for any injury to people or property resulting from any ideas, methods, instructions or products referred to in the content.